EEET ECOLOGICAL ENGINEERING & ENVIRONMENTAL TECHNOLOGY

Ecological Engineering & Environmental Technology 2023, 24(9), 130–149
https://doi.org/10.12912/27197050/173510
ISSN 2719-7050, License CC-BY 4.0

Received: 2023.09.30
Accepted: 2023.10.15
Published: 2023.11.15

Development of a Sustainable Solar Water Desalinator Using a Novel Hollow Hemispherical Grid Shell Solar Selective Absorber Designed via Phasor Particle Swarm Algorithm

Oussama Gliti[1*], Mohammed Igouzal[1],Mohamed Chafik El Idrissi[2]

[1] Laboratory of Electronic Systems, Information Processing, Mechanical, and Energy, University Ibn Tofail, Kénitra, Morocco

[2] Advanced Systems Engineering, ENSA , Kentia , Morocco

* Corresponding author's e-mail: oussama.gliti@uit.ac.ma

ABSTRACT

In this pioneering work, we propose a manufacturing plan for a 3D hollow hemispherical solar selective absorber (HSSA). The HSSA stands out as a superior choice compared to planar absorbers, thanks to its numerous benefits and wide-ranging applications, particularly in solar harvesting and photothermal desalination. Importantly, HSSAs reduce radiative losses by emitting thermal radiation along their curved surfaces, which enhances concentration ratios and minimizes these losses. This study addresses the intricacies of fabricating the HSSA's 3D convex shape. Our approach draws inspiration from a set of 2D flat solar selective absorbers (SSAs), each fine-tuned to adapt angles and intensities in response to solar radiation. These optimized SSAs are then arranged within a grid shell framework. As an illustrative example, we consider the widely-used selective coating W/Al_2O_3-W/Al_2O_3. We optimize parameters, including layer thicknesses and the incorporation of metal in the absorber, to attain optimal values for photothermal conversion output under varying oblique incidence angles. For this optimization process, we employ the non-parametric particle swarm algorithm known as 'phasor,' recognized for its autonomous search for global optima in complex and multimodal optimization problems. Our calculations yield a remarkable photothermal conversion efficiency, reaching up to 0.966429. This research is driven by the aspiration to maintain such high efficiency, even in the face of fluctuations in solar radiation incidence and intensity throughout the day. Simplifying calculations, we divide the hemisphere into five spots, optimizing each for peak performance according to its positioning. These collective efforts and innovations culminate in the development of a compact solar water desalination system, engineered for efficient operation, even in the presence of one sun.

Keywords: solar selective absorber, interfacial solar steam generation, water desalination, phasor particle swarm optimization algorithm, sustainable development.

INTRODUCTION

Water is an indispensable component for sustaining life, and its significance in our everyday existence cannot be emphasized enough. It plays a fundamental role in numerous aspects of human life, encompassing our well-being, the functioning of ecosystems, and the prosperity of economies. However, the global concern of water scarcity is increasingly prevalent, posing challenges to agricultural practices by limiting the ability to irrigate crops and potentially leading to reduced agricultural productivity. Currently, an estimated 3.5 million people lose their lives annually due to inadequate access to clean water and sanitation facilities, highlighting the critical importance of water as an essential global resource. In Figure 1, a visual representation is provided, illustrating the projected levels of water stress at the national level for the year 2040 (Ahmed et al., 2019). It is noteworthy that merely 2.5% of this water constitutes freshwater. Meeting the growing demand for freshwater is accompanied by significant obstacles due to the rapid expansion

of human civilization (Song et al., 2022). The utilization of desalination technology is crucial for guaranteeing water and food security, but traditionally, it has relied on fossil fuels for energy, making it a highly energy-intensive process. This reliance on fossil fuels has had severe implications, including a significant rise in global greenhouse gas emissions and the depletion of finite fossil fuel resources. Additionally, the environmental impact of desalination extends to the discharge of brine into the ocean, resulting in adverse effects on marine life and ecosystems(Younis et al., 2022).

In the last quarter-century, there has been a notable upswing in research and advancements in utilizing solar energy for desalination purposes. This trend is clearly reflected in the substantial increase in the number of publications focused on this specific area. Solar desalination involves harnessing solar electricity, either directly or indirectly, to facilitate the evaporation of a saline solution, followed by the condensation of the resulting vapor. Essentially, solar distillation combines humidification and dehumidification within a system driven by solar energy.

Solar desalination technology offers a practical and sustainable solution for providing clean drinking water. A meticulously designed solar desalination system has the capacity to supply a substantial amount of purified water to communities, effectively tackling the challenge of water scarcity. This process closely mirrors the natural hydrological cycle, where water vaporizes from liquid surfaces, gets carried by the wind, and eventually condenses and falls as precipitation. In the context of solar stills, vapor condenses on cooler surfaces within the still (Alhaj & Al-Ghamdi, 2019) (Choong et al., 2020). Conventional solar stills are uncomplicated devices that utilize the greenhouse effect to trap heat when exposed to sunlight. This heat, in turn, warms the stored feedwater inside the device, thereby boosting its rate of evaporation. The efficiency and productivity of a solar still are significantly influenced by its design.

The configuration of a solar still has a direct impact on its water-holding capacity. A solar still with a larger surface area can store a greater volume of water and consequently produce more distilled water. However, a larger surface area also entails higher heat loss, potentially diminishing the overall effectiveness of the solar still. Therefore, it is essential to tailor the design of the solar still to strike a balance between surface area and heat loss (Younis et al., 2022). The design of the solar still also significantly influences the ease of its construction and maintenance. A solar still with a simple and uncomplicated configuration is more straightforward to build and maintain compared to a complex one. Consequently, refining the design of the solar still is crucial to find the right equilibrium between efficiency and the ease of both construction and maintenance (X. Li et al., 2022). A well-optimized solar still should maximize its absorption of solar radiation to enhance its efficiency. For instance, research has shown that pyramidal or hemispherical forms are more efficient in this regard than other configurations.

The concept of an interfacial solar steam generator (ISSG) has emerged as a solution to enhance the efficiency of solar evaporators that utilize solar energy at the water's surface. ISSGs are designed to promote energy conversion and water evaporation precisely at the interfaces of a

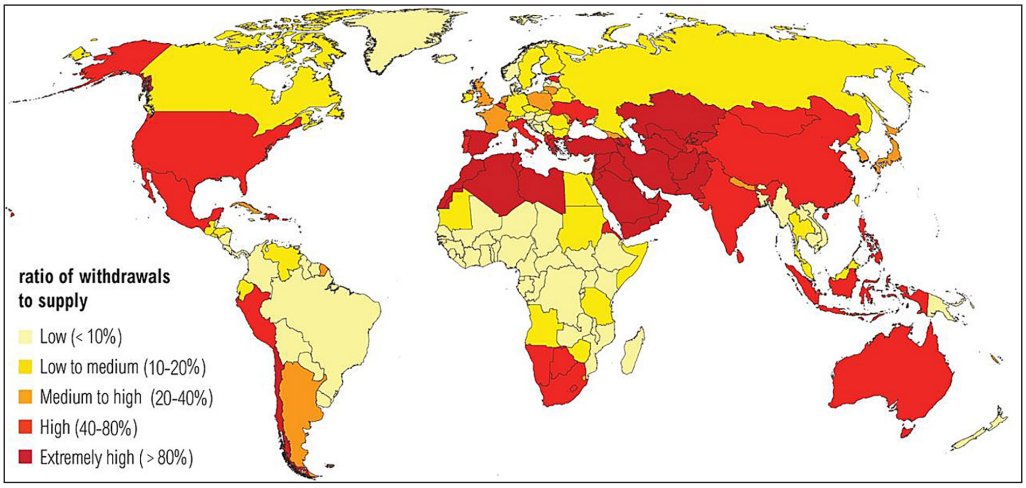

Figure 1. Water stress by Country 2024 (Luo et al., s. d.)

solar evaporator. Typically, an ISSG consists of two key components: a photo absorber, a material known for its ability to efficiently absorb sunlight, and a porous substrate that enables water evaporation. The photo absorber harnesses solar radiation, converting it into heat energy, while the porous substrate allows for direct contact between water and the photo absorber, thereby facilitating the evaporation process effectively.

These materials are not specially created for solar absorption and heat conversion, which results in numerous limitations, they are not optimized for high solar absorption. Consequently, they do not efficiently catch and convert incoming solar light into thermal energy. these materials are often not appropriate for generating and maintaining the high temperatures necessary for effective steam production. While these materials can be utilized for basic and low-cost experimental setups or in circumstances where high efficiency is not the major issue, they are not good alternatives for interfacial solar steam generators that require constant and effective heat absorption and conversion. In contrast, solar selective absorbers (SSA) are an artificial material which are developed to optimize sun absorption, decrease heat loss, and operate at high temperatures, making them more ideal for efficient and dependable steam generation from solar energy. Also SSAs have high absorption in the solar spectrum [300–2500] nm and low emission in the infrared range [2500–25000] nm, compared to black bodies who have high spectral absorption, but at the same time they possess high emissivity, especially at high temperature, as it is shown on Figure 2, the SSA characterization facilitates maximizing solar energy absorption and minimizing heat radiative loss, thus improving the overall photothermal conversion efficiency of SSAs (J. Zhang et al., 2022),

Efficient solar selective absorbers (SSAs) are a rarity in nature, as their name implies. These intelligent surfaces or film materials are typically achieved through the creation of photonic metamaterials or metasurfaces designed to effectively capture the entire spectrum of sunlight while reflecting infrared (IR) light to prevent thermal radiation heat loss. Without the utilization of such selectively absorptive materials, generating high-temperature steam under the illumination of one sun for specific applications like water boiling (>100 °C), sterilization (120°C), and photothermal catalysis (299°C) (J. Zhang et al., 2022; Y. Li et al., 2021) is often challenging, if not impossible.

The efficiency of a solar selective absorber relies on a multitude of factors. These include material selection, the absorber's shape and structure, encompassing considerations such as the quantity and thickness of its layers, the point at which sunlight strikes it, and the concentration of solar energy. Solar absorption tends to be greater

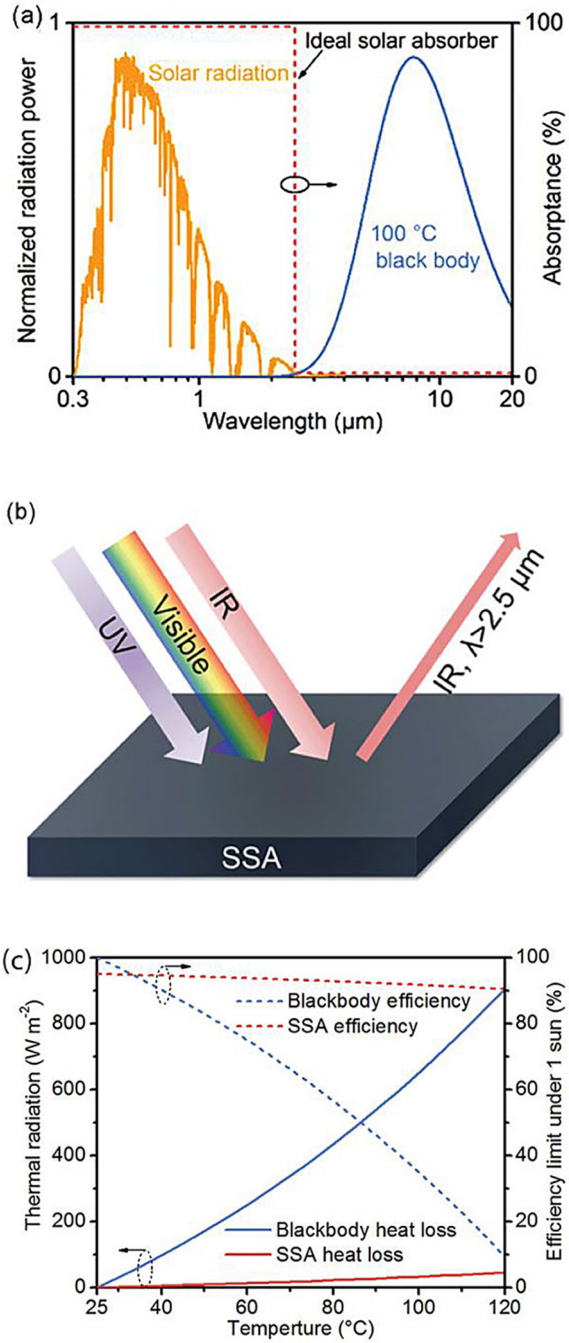

Figure 2. (a) AM1.5 G solar spectrum, absorption spectrum of the ideal SSA, and radiation spectrum of 100 C blackbody; (b) schematic of the SSA; (c) heat radiative loss and photothermal conversion efficiency of blackbody absorber and commercial SSA under 1 sun. Reproduced with permission (Li et al., 2021)

when sunlight hits the absorber at a perpendicular angle and tends to diminish as the incident angle increases. To enhance its efficiency, the absorber's design must consider the angle of sunlight incidence. The specific design and materials employed for the solar selective absorber will be tailored to meet the desired attributes and intended applications of the absorber.

In this study, we aim to enhance the performance of the solar selective absorber by changing its geometry. Specifically, we propose the adoption of a hemispherical shape for the absorber, which offers significant advantages over a flat or planar surface. The hemispherical configuration has the potential to greatly enhance the concentration factor and ensure more uniform solar radiation distribution across its surface. This design provides a full 360-degree exposure to sunlight throughout the day, eliminating the necessity for mechanical tracking mechanisms. Moreover, this three-dimensional structure facilitates improved solar tracking without the need for manual adjustments or mirror tracking systems. Contrary to this, flat plate absorbers are typically two-dimensional and have a limited surface area exposed to sunlight at any given moment. Their efficacy declines when the angle of incidence deviates from normal (perpendicular). Planar absorbers are highly reliant on the angle of incidence of sunlight, and they are most effective when sunlight is directly perpendicular to the surface. Hemispherical absorbers tend to have lower radiative losses because they emit thermal radiation along a curved surface, which might result in more complicated radiative heat transfer patterns. This design provides for improved trapping of heat inside the absorber and lowers the leakage of thermal radiation to the surroundings. The curved curvature of the absorber may be employed to produce a vacuum-insulated chamber. The vacuum may function as a good insulator by decreasing heat transmission via conduction and convection.

However, the complexity and cost associated with manufacturing hemispherical absorbers, owing to their three-dimensional shape, present a challenge. Ensuring a consistent coating thickness and uniform properties across the entire hemispherical surface is essential for efficient absorption and minimal heat loss. Maintaining this uniformity can pose significant technical demands, particularly on a large scale. Transforming a 2D flat plate design into a 3D hemispherical solar selective absorber can be accomplished through a process referred to as "forming" or "shaping." However, scaling up this process to meet the extreme demands and versatility required for various applications, such as power generation, agricultural greenhouse heating, medical sterilization (e.g., solar autoclaves), and especially desalination of seawater or brackish water, presents substantial challenges. Nevertheless, the potential of this technology in providing solutions for drinking water, agriculture, and industrial processes underscores its significance and value.

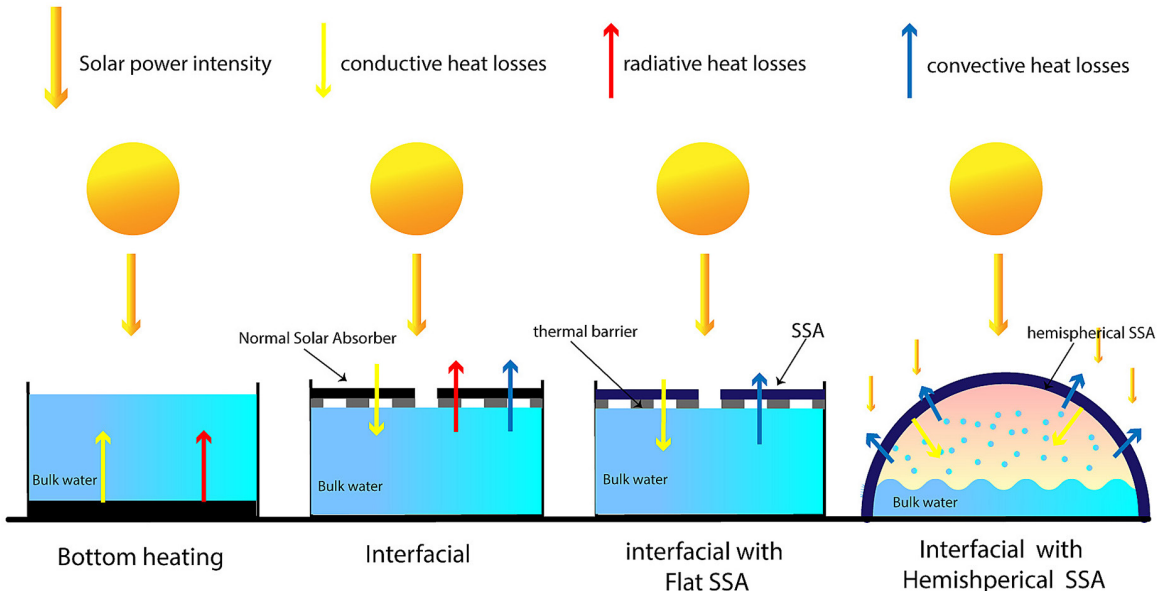

Figure 3. Representation of different materials and shape used on ISSG, our proposed (HSSA) and represent the solar radiative power, conductive, convective, and radiative loss

In light of the challenges associated with this impeccable design, this study aims to establish a theoretical framework for the construction and production of a hemispherical-like hollow Solar Selective Absorber (SSA) design. This innovative design is founded upon a grid shell framework, which constitutes an expansive structure comprising an interconnected lattice of trapezoidal flat plate SSAs. As illustrated in Figure 4, each of these flat plate SSAs undergoes optimization both in terms of its shape to accommodate intricate architectural forms and its optical properties to maximize photothermal efficiency during daylight hours. The proposed design optimization entails determining the optimal distribution of flat SSAs within the grid shell to attain the desired photothermal efficiency. Each grid element interacts with solar radiation characterized by specific intensity and incidence angles. Our endeavor is to identify the precise parameter combinations that enhance the efficiency and performance of each flat SSA's distribution, aligning them with the sun's position and beam incidence.

Furthermore, the widespread adoption of improved selective absorbers/emitters faces obstacles due to the high production expenses associated with them. With the exception of certain inherent materials, most selective absorbers/emitters reliant on nanophotonic structures necessitate manufacturing through intricate high-vacuum deposition processes or nanofabrication techniques in controlled environments like PVD, CVD, e-beam lithography, and reactive ion-etching. Since the optical characteristics of these nanostructures are notably sensitive to factors such as film thickness, nanoparticle dimensions, and pattern feature sizes at the nanoscale level, crafting high-performance and durable absorbers/emitters can be quite challenging. Hence, optimization becomes a crucial phase in enhancing the efficiency of solar selective coatings, eliminating the need for numerous trial-and-error approaches. By maximizing their capacity to absorb solar radiation and minimizing thermal emittance, optimization efforts can identify the most suitable materials and processes tailored to specific operational conditions, such as temperature and solar radiation intensity. However, a significant challenge in our context is the abundance of parameters that need optimization, and deterministic methods often prove inefficient given the presence of local optima. As a result, we have chosen stochastic approaches to address this challenge (Ajdad et al., 2019).

Simulation methods and theoretical background

We will begin our study by using a flat plate SSA as a model. We'll determine which of its parameter values perform well, including the thickness of the three layers, the anti-reflection coating, the absorber-doped layer, the IR reflective back layer, and the presence of metal inclusions. We will also take the angle of incidence into consideration. Our analysis will encompass the response variation from near-normal incidence to oblique incidence. By examining how the response changes as the angle of incidence

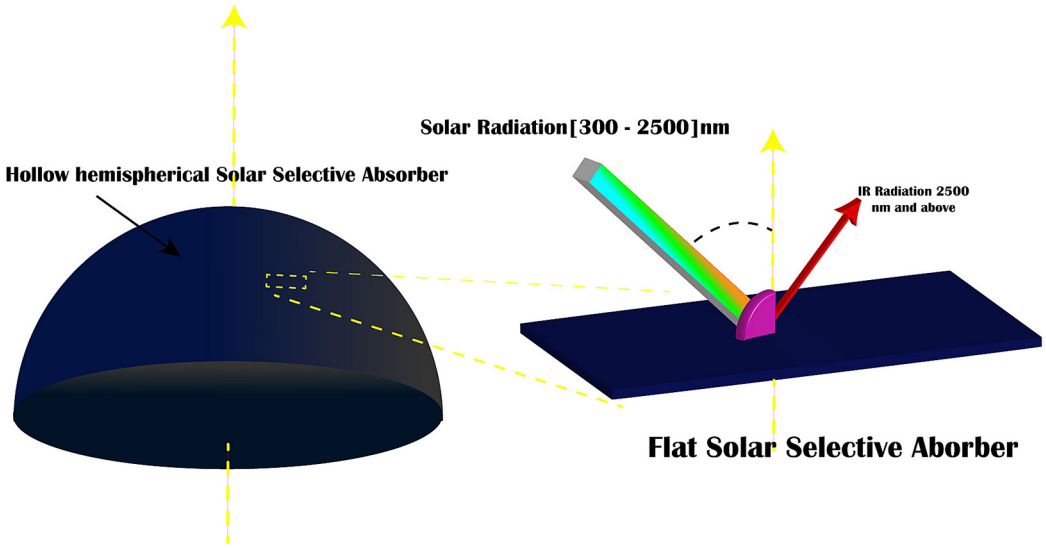

Figure 4. Development of the hemispherical solar selective absorber based on a 2D flat plate

deviates from the normal, we can gain valuable insights into the behavior of the system under different conditions of azimuthal solar angle variation, from noon until the decrease in sun intensity, considering the real received solar energy flux of SSA at oblique incidence reduces to cos(θ) times (Wu et al., 2022). Taking into account our use of W/W-Al_2O_3/Al_2O_3, where tungsten (W) serves as the infrared reflector and metallic inclusions are found in the cermet, while aluminum oxide (Al_2O_3) functions as the antireflective layer and matrix ceramic in the W-Al_2O_3 cermet, it's worth noting that this architectural configuration has been adopted in a commercially available solar absorber as reported by (K. Zhang et al., 2017). Other research studies have explored variations, such as the W-Al_2O_3 graded cermet layer structure with a gradient of metallic increments, with higher inclusions in the second layer. Additionally, some studies have proposed the inclusion of a barrier layer between the second cermet layer and the reflective back layer to prevent thermal inter-diffusion (X. Wang et al., 2017). In our specific case, we have chosen to employ a single cermet structure to reduce computational expenses. This decision aligns with the intended application of the solar selective absorber, which operates at moderate temperatures not exceeding 120°C. This temperature range does not necessitate a more complex structure with specialized materials.

Coatings after fitting the optical properties of those materials, and knowing the variation of each wavelength, the data was taken from Palick data base (L.-Y. Chen, 2021), we can conclude the complexes refractive index N(λ) = n + ik of each material, The spectral complex refractive indices of the W–Al_2O_3 composite layer were estimated by applying an Effective Medium Approximation (EMA) method (Yu et al., 2015). spectral reflectance R(λ) can be calculated using a conventional method based on Fresnel equations, known as the Transfer Matrix Method (TMM), detailed in the literature (L.-Y. Chen, 2021).

The stack produces an optical cavity with metal-dielectric graded index solar, it must have the capability of confining the light by numerous reflections and producing resonators owing to the effects of interference.is intended to have a specified thickness and refractive index of each layer, so that the reflected waves from various layers destructively interfere with each other at the appropriate wavelength. This leads in substantial absorption of the incident solar energy at that wavelength, while the reflected light at other wavelengths is reduced.

The efficacy and the spectral selectivity of a solar absorber is evaluated by the solar absorptance and thermal emittance, solar absorptance as must be estimated. AS represents the ratio of solar flux density (in W/m^2) absorbed by the absorber over the flux density receives from the Sun(Ning et al., 2020), otherwise the thermal emittance is the ratio of the irradiance emitted by the absorber at the operating temperature T_a, compared to the irradiance of an ideal blackbody at the same temperature (Grosjean et al., 2021), The spectrally averaged hemispherical solar absorptance α(θ) and radiative emittance ε(θ) are defined by:

$$\alpha(\theta) = \frac{\int_{0.3\mu m}^{2.5}(1-R(\theta,\lambda))I_S(\lambda)d\lambda}{\int_{0.3\mu m}^{2.5} I_S(\lambda)d\lambda} \quad (1)$$

$$\varepsilon(\theta, T) = \frac{\int_{2.5\mu m}^{25\mu m}(1- R(\theta,\lambda))I_b(\lambda,T)d\lambda}{\int_{2.5\mu m}^{25\mu m} I_b(\lambda,T)d\lambda} \quad (2)$$

where: $I_s(\lambda)$, $I_b(\lambda, T)$ and $R(\theta, \lambda)$ – respectively the solar radiation spectrum, blackbody radiation spectrum at T_a, and the angular reflectance spectrum of the solar absorber.

The solar spectrum $I_s(\lambda)$, taken as a reference for calculation is the standard ASTM G173-03 Direct and Circumsolar (DC) AM1.5 spectrum, and the is Planck's law at T_a. The absorber solar flux density is deduced from spectral absorptance $\alpha(\theta) = (1 - r(\theta, \lambda)$, weighed by the solar spectrum $I_s(\lambda)$ and integrated over wavelength λ (Grosjean et al., 2021), The total irradiance emitted by the absorber at T_a, is calculated by integrating over wavelength its spectral emittance $\varepsilon(\theta) = (1 – R(\theta, \lambda)$ weighed by the blackbody spectral irradiance at T_a (Eq. 4) (Grosjean et al., 2021). We adopted the calculation method proposed by (Duffie & Beckman, s.d.) in which the data that are available are measurements of monochromatic reflectance. The optical performance of SSA is characterized by the efficiency of their solar-thermal conversion process, Our goal, and It is the ratio of absorbed solar flux density, minus the radiative thermal losses divided by the total concentrated solar flux density received by the absorber, convective and conductive thermal losses are also present for real thermal absorbers, but they are neglected here compared to much higher radiative losses which is simply defined as:

$$\eta_{solar-th} = \alpha(\theta) - \varepsilon(\theta, T)\frac{\sigma({T_a}^4 - {T_0}^4)}{CI_S\eta_{opt}} \quad (3)$$

where: $\eta_{solar\ -\ th}$ – depends on the absorber optical performance $\alpha(\theta)$ and $\varepsilon(\theta, T_a)$, the collector concentration ratio (C), the thermal absorber and the ambient temperatures (respectively T_a and T_0), the solar irradiance I = 900 W/m^2 for ASTM-G173DC) and the concentrator (mirror) optical performance (η_{opt}), which are both derived from spectral reflectance R(θ, λ).

The aim of this work is finding the optimal and most suitable parameters inputs to maximize this value and achieve higher conversion and yield (Grosjean et al., 2021), we will consider it as being our main objective function, the absorber must have a low spectral reflectance in the solar spectral domain (300–2500 nm – higher absorptance) which means the disappearance of electromagnetic radiation inside the medium and happens when the incident photon's energy is equal to the material band gap (B. Liu et al., 2021), in other words, the cut-off wavelength of an ideal SSA with a step function spectrum should be 2500 nm for the target applications at 100°C under 1 sun. The cut-off wavelength is a critical parameter in the design of SSAs, which highly relies on both the solar concentration ratio C and the operating temperature T_a. The reflectance must be higher below this wavelength in infrared domain (2500–30000 nm). Due to its extreme value and requirement and its versatility in different application, such as Power generation, in Agriculture in greenhouse Heating, in medical Sterilization it can behave as a solar Autoclaves, and specially in can be used for desalinating seawater or brackish water, making it suitable for drinking, agriculture, and industrial processes.

To address the specific problems related with this flawless design. In this study, we will give a theoretical notion of how to build and produce hemispherical-like hallow SSA design, based on grid shell framework comprising a long span structure consisting of a lattice of single interconnected flat Plate trapezoidal SSA, each One of this flat plat SSA distributed in this system are topologically optimized by their shape to fit this complex architectural shapes, and their optical properties to reach a maximum photothermal efficiency , based on the solar path During daytime hour. The proposed Topology optimization comprise of determination of an optimal distribution of flat SSA within the grid shell to achieve a desired photothermal efficiency, each element of the grid will confront the sun radiations with specific intensity and incidence angle, we will endeavor to identify the proper parameters recipe to increase the efficiency and performance of each flat SSA distribution to match the right sun location and beam incidence.

As well, large-scale deployment is hindered by high fabrication costs of current improved selective absorbers/emitters. Except for some intrinsic materials, most of the selective absorbers/emitters based on nanophotonic structures have to be manufactured by sophisticated high-vacuum deposition procedures or nanofabrication techniques in clean rooms, such as PVD, CVD, e-beam lithography, and reactive ion-etching. Since the optical properties of these nanostructures are particularly sensitive to the film thickness, nanoparticle size, and pattern feature size at the nanoscale level, it is relatively tough to create high-performance and robust absorbers/emitters.

Reasons why optimization is important crucial phase to improve the efficiency of solar selective coatings, and to avoid multiple trial and error process, by maximizing their ability to absorb solar radiation and minimize their thermal emittance, can help to reduce the cost of manufacturing solar selective coatings by identifying the most effective materials and process that are adapted to specific operating conditions, such as temperature and solar radiation intensity. On the other hand, the great number of parameters to optimize is among the challenges encountered in our scenario where the deterministic approaches are often inefficient considering the presence of local optimums. For this reason, we opted for stochastic approaches (Ajdad et al., 2019)

Optimization strategy

Here we encounter an optimization problem with 5 dimensions, with strongly nonconvex discontinuous nature of the objective functions, Therefore, metaheuristic algorithms are valuable tools for this case, because of their ability to handle complex, nonlinear, and global optimization problems without the need for derivatives. They offer flexibility, adaptability, and effectiveness in a wide range of optimization scenarios, making them a valuable choice in many practical applications. metaheuristics can explore a broader range of solutions and have a better chance of finding the global optimum. The search for the optimum goes through the use of global and non-local optimization methods. Methods such as genetic

algorithms, artificial neural networks, ant colony algorithms, particle swarm optimization (PSO), Simulated Annealing (SA) and others.

The most extensively used method for optimizing a solar selective absorber is the Genetic method (GA), the widespread usage of genetic algorithms in optimizing solar selective absorbers. The flexibility, efficiency, and capacity to tackle complicated multivariable issues make genetic algorithms a popular choice for academics in the field. This technique has been extensively employed in numerous research papers for solar selective absorber design and optimization. a multi-island evolutionary algorithm was utilized to improve the configuration of an SSA micro-nano structures with manufacturability for thermal and energy applications (W.-W. Zhang et al., 2021), a genetic algorithm was employed to optimize the optical performance of a metamaterial-based solar thermal absorber (Cai et al., 2021). For enhancing the solar photothermal conversion efficiency of a nano-thin Cr film, a global optimization technique based on a genetic algorithm was devised (Wang et al., 2020). Genetic algorithms offer a powerful and flexible approach to optimizing solar selective absorbers. While other optimization methods may have their own advantages, other optimization methods used for solar selective absorber design, Deep learning has been used in combination with multi-objective double annealing algorithms to optimize the design of selective solar absorbers (Ma et al., 2023).

Particle Swarm optimization has gained more interest on this field It is also used in this application due to its simplicity and efficiency; it is beneficial in applications where computational resources or time constraints are a concern, with fewer customizable parameters, strikes a balance between exploration (searching the solution space generically) and exploitation (focusing on favorable spots). This equilibrium is often established naturally through the algorithm's dynamics. Similar to several other optimization strategies, minimizing the demand for extensive parameter change. Looks to perform pretty well across a variety of optimization difficulties without needing extensive problem-specific tailoring. SSA have multiple parameters, and PSO can optimize them simultaneously to achieve the desired performance, it can handle complex multivariable problems and find optimal solutions. broadband (J. Liu et al., 2022) designed highly polarization selective absorber based on the PSO algorithm. Researchers used PSO to design a perfect solar absorber from the visible to the near-infrared band (You et al., 2023) .a temperature self-adaptive ultra-thin solar absorber was designed using an optimization algorithm that included PSO (J. Chen et al., 2023).

PSO is an evolutionary computing approach originally developed by Kennedy and Eberhart (Freitas et al., 2020). It shares fundamental characteristics with evolutionary computation techniques, such as initializing a population of random solutions and iteratively seeking the best possible solutions. Within the PSO framework, candidate solutions, referred to as particles, are steered through the problem space by following the paths of the currently best-performing particles. The inspiration for the concept of a particle swarm was drawn from simulating a simpler social system, with the goal of replicating the graceful and unpredictable movement observed in a flock of birds. Each particle in the PSO algorithm maintains awareness of its location within the problem space, which is associated with the best solution (fitness) it has achieved up to that point, referred to as 'pBest' (personal best). Additionally, a global version of PSO monitors another 'best' value called 'gBest' (global best), which represents the overall best value achieved by any particle in the population and its corresponding position. The fundamental idea behind particle swarm optimization revolves around adjusting the velocity of each particle, propelling it towards its 'pBest' and 'gBest' positions in each iteration, particularly in the global variant of PSO. The updates of the particles are accomplished as per the following:

$$V_{id}^{iter+1} = V_{id}^{iter} + C_1 \times \mathrm{r1}_{id}.\left(pbest^{iter}_{id} - X_{id}^{iter}\right) + C_2 \times \mathrm{r2}_{id}.\left(gbest^{iter}_{id} - X_{id}^{iter}\right) \quad (4)$$

where: *c1* and *c2* – acceleration control coefficients, *r1id* and r2id are random coefficients of two uniform random sequences in the range of (0, 1), and *iter* is the number of current iterations, the values of particles velocity V_i is defined in the range $[^{-}V_{max}, V_{max}]$ to prevent the particles from moving beyond the problem search space (Ghasemi et al., 2019).

In the new iteration, the personal best position of each particle and the global best position of the population are updated as:

$$pbest^{iter+1}_{id} = \begin{cases} pbest^{iter}_{id}, \text{if f}\left(pbest^{iter}\right) \le f\left(X_{id}^{iter}\right) \\ X_{id}^{iter}, otherwise \end{cases} \quad (5)$$

$$Gbest^{iter+1}{}_{id} = \begin{cases} pbest^{iter}{}_{id}, \text{if f}(pbest^{iter+1}) \le f(Gbest^{iter}) \\ Gbest^{iter}, otherwise \end{cases} \quad (6)$$

The PSO method often faces a rapid convergence towards local optima, especially when tackling optimization challenges of increasing complexity and scale. Unlike some other evolutionary optimizers, it may exhibit reduced diversity and precision primarily because of its heavy reliance on algorithmic control parameters. To address these limitations, substantial efforts have been made to enhance the performance of PSO. In this context, this study introduces a distinctive variant of PSO known as Phasor Particle Swarm Optimization (PPSO). PPSO draws inspiration from phasor theory in mathematics. The PPSO method, control variables are modeled using phasor angles θ. This changes PSO to a non-parametric algorithm. The best advantage of PPSO compared to other algorithms is the increased optimization efficiency even with increased problem dimension. the proposed model for particle movement is as follows:

$$V^{iter}{}_i = p(\Theta_i{}^{iter}) \times (\text{Pbest}_i{}^{iter} - X_i{}^{iter}) + g(\Theta_i{}^{iter}) \times (\text{Gbest}_i{}^{iter} - X_i{}^{iter}) \quad (7)$$

In the PPSO algorithm, the phase angle θ lying within a range between 0 and 2π radians, the following function have been selected for PPSO:

$$p(\Theta_i{}^{iter}) = |\cos(\Theta_i{}^{iter})|^{2\sin\Theta_i{}^{iter}} \quad (8)$$

$$g(\Theta_i{}^{iter}) = |\sin(\Theta_i{}^{iter})|^{2\sin\Theta_i{}^{iter}} \quad (9)$$

The adaptive search characteristics of individual particles are shaped by two functions $p(\theta_i^{iter})$ and $g(\theta_i^{iter})$ as described by (Pyone et al., s. d.). The behaviors of these functions during algorithm execution for iterations 1-200 and 1-20 are depicted in Figures 5 and 6, respectively. These functions capture the essential behaviors and techniques employed in the algorithm. There are instances where both functions increase or decrease simultaneously at certain intervals, while at other intervals, their variations are opposite. This approach achieves a balance between global and local search, transforming the algorithm into an adaptive and nonparametric one. The PPSO algorithm's flowchart is illustrated in Fig. 8. N random particles represented as $\vec{X}^1{}_i = |X^1{}_i| < \Theta_i{}^1$ are generated. Each particle consists of a D-dimensional magnitude vector $X^1{}_i$, a scalar phasor angle θ_i^1, and an initial speed limit $V^{iter=1}{}_{max,i}$. These values are generated using a uniform random number generator. Subsequently, the particle's position is updated utilizing the following Equation:

$$\vec{X}^{iter+1}{}_i = \vec{X}^{iter}{}_i + \vec{V}^{iter}{}_i \quad (10)$$

The determination of the personal best (Pbest) and global best (Gbest) positions follows a process similar to that of the original PSO algorithm:

$$\Theta_i{}^{iter+1} = \Theta_i{}^{iter} + |\cos\Theta_i{}^{iter} + \sin\Theta_i{}^{iter}| \times 2\pi \quad (11)$$

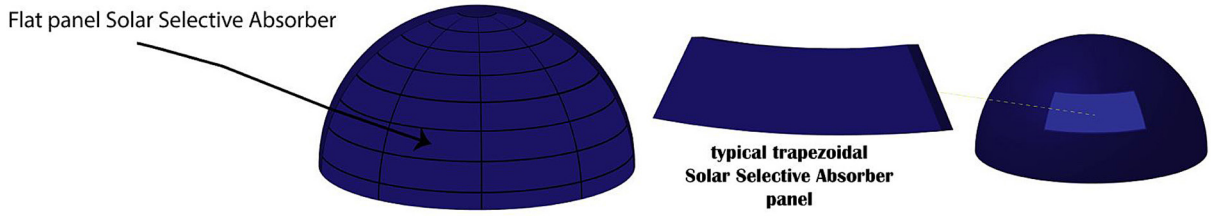

Figure 5. Grid shell distribution of the hemispherical solar selective absorber

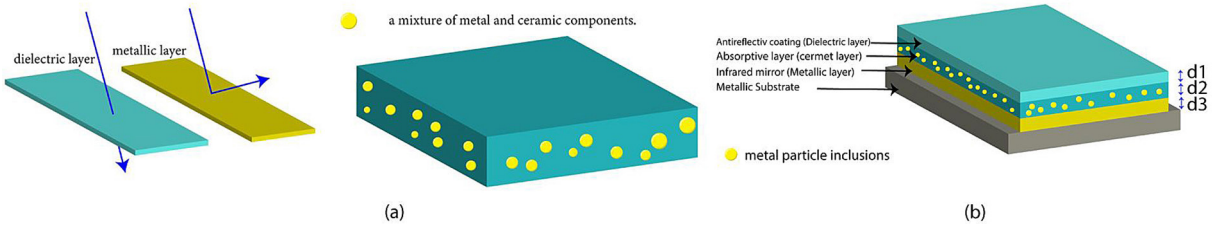

Figure 6. (a) Cermet layer containing a metallic inclusion embedded into dielectric materials (b) The absorber layer, W-Al_2O_3, sandwiched between an IR reflective layer, W, and the anti-reflective layer, Al_2O_3

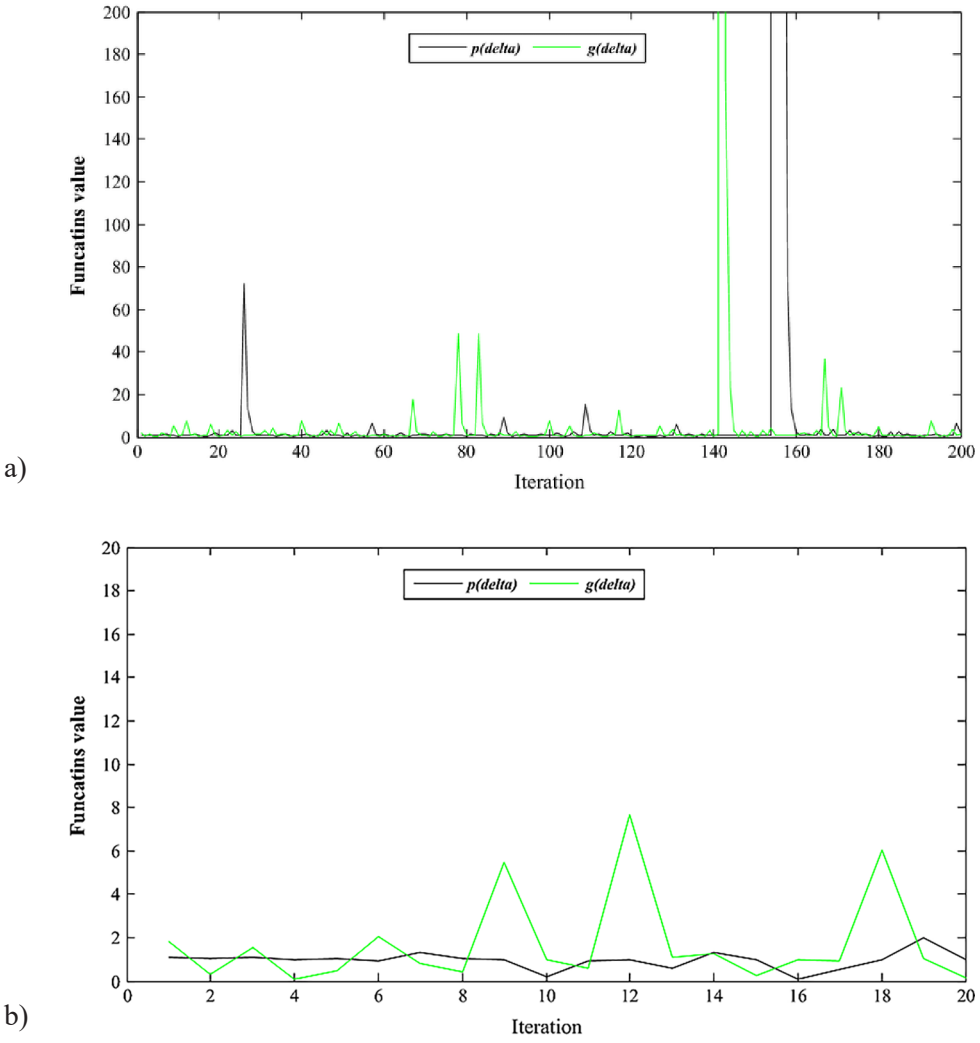

Figure 7. Typical values of functions $p(\theta_i^{iter})$ and $g(\theta_i^{iter})$ in PPSO algorithm based on the typical changes of the phase angle θ_i of *i*th particle (Ghasemi et al., 2019); (b) iterations 1-20

$$V_{i,max}^{iter+1} = W(\Theta) \times (X_{max} - X_{min}) = |\cos(\Theta_i^{iter})|^2 \times (X_{max} - X_{min}) \quad (12)$$

The effectiveness of the PPSO algorithm we propose is evaluated by comparing it to other enhanced PSO methods. We examine their respective contributions to improvement and the settings of their parameters, as detailed in the Table 1.

RESULTS AND DISCUSSION

To gain insights into the behavior of the objective function, which depends on the choice of parameters $d_{Absorber}$, d_{AR} and the (metal volume fractions), we have constructed a 3D contour plot. By holding one parameter constant and varying the other two, we observe that solar thermal efficiency exhibits a similar behavior to solar absorbance. In fact, under the assumption that emission and radiative losses are negligible, we can consider these two quantities to be nearly identical.

The maximum efficiency is consistently found at a thickness of approximately 100 nm for both parameters, suggesting that there is no need for the thickness to exceed this value, especially in the range of 50–100 nm for both thickness values (Grosjean et al., 2018). This behavior is a result of the creation of destructive interference at the interfaces between the layers, ensuring the absorption of a significant portion of incident radiation while minimizing heat losses.

However, it's important to note that an increase in both thickness parameters leads to a rise in emission values, as depicted in Figure 4. Despite this increase in emission, our optimization goal is to identify a critical parameter value at which the yield remains significantly high.

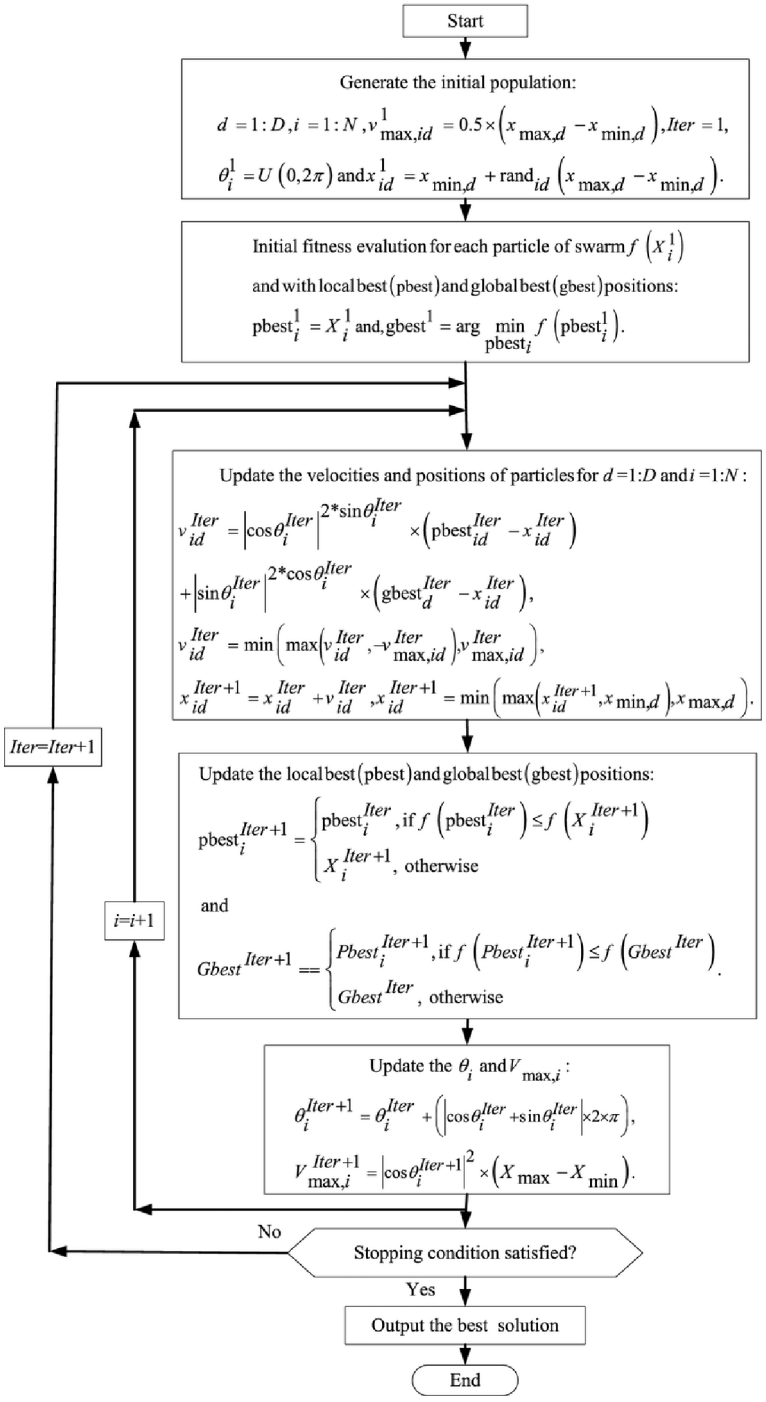

Fig. 8. Flowchart of PPSO (Ghasemi et al., 2019)

Additionally, as shown in Figure 6 and in accordance with Equation 3, an increase in absorber temperature and concentration ratio leads to an improvement in the efficiency of our solar selective absorber.

To meet our physical requirement, the solution obtained by the phasor optimization algorithm must be feasible and physically meaningful, reason why imposing bounds or constraints while employing metaheuristic optimization is important for this reason, other reason is reduce the search space, our boundaries employed are demonstrated on Table 2, this calculation is done by in house python code, the optimization part was done by the programming tool MEALPY python library (Van Thieu & Mirjalili, 2023). Also, the population size was set to 50 particles for all adjusted particle swarm's algorithms, which is the widely used, and number of iterations is set to 100. Table 3 show the results of the objective

functions and the value of the decisional parameters of the algorithm carried out, after running all the optimization algorithm PPSO and all the other 4 of other PSO variant, the winning algorithm (CL-PSO, PPSO) shows a solar thermal value greater than 0.96 with very slight difference, already found by the original one.

Regarding convergence as shown in Figure 9 the PPSO explore quickly in some few iterations, and can achieve the Global minima in the early stage of the optimization process, unlike other algorithms which took a lot of calculation and iteration time to reach the maximum, the value of the objective function keeps changing during iteration, proven that the algorithm deals well with the problem landscape, which can allow to close the calculation in fairly limited iterations and reduce the calculation cost and running time.

The value of the decisional parameters is almost equal, the thickness of the first antireflective layer is approximately d_{AR} = 48–50 nm which represents the first contact and receives solar radiation, its role is to absorb as much solar radiation as possible with this optimal value. regarding the value of the absorber $d_{absorber}$ and the metal inclusion, which is a major and important layer in the multistack, this value makes it possible to confine the wavelength of the solar rank, the absorber layer tends towards the values of 45.77 nm and the metal volume fraction is 34% which means that leaving only 66 of the dielectric property in the layer, the two values allow to tune the selectivity inside the layer, which allows the process of destructive interference to be carried out. For the thickness of the Infrared metallic layer, it doesn't have much influence, since its unique role is to reflect infrared radiation, provided it is not minimal enough, regarding the angle of incidence the algorithm confirms that it should be as close to normal as possible, in our case it takes the minimum value 5°.

The Figure 15 shows the reflection response of all the optimization PSO algorithms, the variation of the two algorithms PPSO and CL-PSO is almost the same, their curves are almost identical, this is the maximum value available for this design, he tries as much as possible to be at his minimum in the solar rank, the transition after the cutoff wavelength is not rough enough, as the ideal case. The configuration or recipe found by our algorithm performs well, and gives a maximum value only on a near normal incidence, reflection increases with very high incidence values, which automatically means a reduction in absorption, as can be seen in the Figure 9 numerous variables need to be addressed, such as the material composition, surface morphology, and design of the coating. The material exhibits a low reflectivity, measuring less than 10%, across a wide wavelength range of 300 to 1500 nm when subjected to incident angles ranging from 5° to 60°. As the incident angle rises from 65° to 85°, there is a gradual increase in reflectance, and this shift is accompanied by a change in the transition wavelength. The quasi-optical cavity structure allows for multiple absorption mechanisms, encompassing thin film interference and the plasmonic absorption of metal nanoparticles within the cermet layer. The light that is reflected can experience interference phenomena as a result of the numerous reflections taking place within

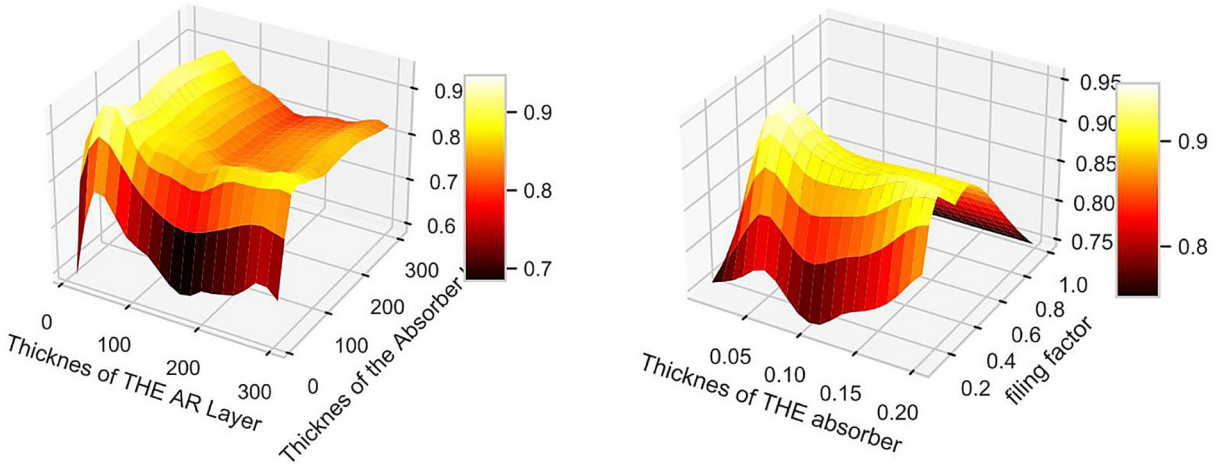

Figure 9. Variation of the $\eta_{solar-th}$ efficiency of the SSA depending on (a) $d_{Absorber}$ & d_{AR} (b) $d_{Absorber}$ & metal volume fractions variation

Table 1. A brief description of the proposed PSO variants and their parameter settings

Year	PSO Variant	Contribution	Improvement	Inertia weight and acceleration coefficient	Values given in our case
1998	Original PSO (PSO-*ω*) (Freitas et al., 2020)	The inertia weight ω was proposed to make a balance between local and global search	The added inertia weight parameter has been shown to improve the convergence rate and accuracy of the algorithm	$w^{iter} = w_{max} - (w_{max} - w_{min}) \times \frac{iter}{iter_{max}}$	$C_1 = 2.05$ $C_2 = 2.05$ W_{min}= 0.4 $W_{max} = 0.9$
2005	C_PSO (Xia & Li, 2020)	Combining PSO with chaos is to use an adaptive inertia weight factor (AIWF) that is built on a chaotic sequence [ref]	Combining PSO with chaos theory is a promising method for improving the performance of PSO and creating effective and efficient optimization algorithms. The use of adaptive inertia weight factors and linear decreasing and chaotic inertia weights are two methods that have been suggested to achieve this goal.	$\omega = \begin{cases} w_{min} + \frac{(w_{max}-w_{\min})(f-f_{min})}{f_{avg}-f_{min}}, f \le f_{avg} \\ w_{max}, f > f_{avg} \end{cases}$ *f* is the current objective value of the particle, f_{avg} and f_{min} are the average and minimum objective values of all particles, respectively.	$C_1 = 2.05$ $C_2 = 2.05$ W_{min}= 0.4 $W_{max} = 0.9$
2004	HPSO-TVAC (Ghasemi et al., 2017)	The HPSO-TVAC algorithm uses time-varying acceleration coefficients (TVAC) to adjust the acceleration coefficients during the optimization process, which improves the algorithm's performance	TVAC alters the acceleration coefficients during the optimization process, which helps the algorithm converge to the ideal solution faster and with more accuracy	$\omega^{iter} = 0$ $C_1^{iter} = C_1^{iter=1} - (C_1^{iter=1} - C_1^{iter_{max}}) \times \frac{iter}{iter_{max}}$ $C_2^{iter} = C_1^{iter=1} + (C_2^{iter_{max}} - C_2^{iter=1}) \times \frac{iter}{iter_{max}}$	C_i = 0.5 $C_f = 0$
2006	CL_PSO (Lin & Sun, 2018)	Utilizes a new learning strategy to improve the performance of PSO on complex multimodal problems has been shown to improve the convergence speed and quality of the global optimal solution, performance is affected by the learning proportion P c, which can be adjusted to achieve better performance on different problems	The CLPSO algorithm is a promising approach for global optimization of multimodal functions. Its new learning strategy, local search, and adjustable learning proportion are key features that distinguish it from other PSO algorithms	$w^{iter} = w^{iter=1} - (w^{iter=1} - w^{iter_{max}}) \times \frac{iter}{iter_{max}}$	$C_{local} = 1.2$ C_{global}= 0 W_{min}= 0.4 W_{max}=0.9 max_flag = 7

Table 2. Lower and upper bound of the decision parameter for the optimization process

Parameter	Lower band	Upper band
d_{Ar}	10 nm	200 nm
$d_{absorbent}$	10 nm	200 nm
$d_{IR\ reflecter}$	10 nm	200 nm
Metal inclusion (M.I) %	10 %	100 %
Incidence angle	5°	90°

Table 3. Value of the objective function found for the different PSO variant proposed algorithms for 50

PSO Variant	Parameters values					Fitness value
Original-PSO	d_{ar}	$a_{absorber}$	$d_{IR\ reflector}$	Mi (metal inclusion)	Ia (incidence angle)	0.9600243363528834
	0.04937616	0.03974237	0.08764281	0.33510812	13.14241752	
CPSO	d_{ar}	$a_{absorber}$	$d_{IR\ reflector}$	Mi	IA	0.9057124936405047
	0.06945932	0.05293485	0.07846527	0.3541672	31.87225407	
CPSO	d_{ar}	$a_{absorber}$	$d_{IR\ reflector}$	Mi	IA	0.9419535675423053
	0.05232107	0.1999882	0.06323489	0.25551808	5.00745501	
CPSO	d_{ar}	$a_{absorber}$	$d_{IR\ reflector}$	Mi	IA	0.9671620746678763
	0.04941893	0.04526404	0.06551798	0.349769	5	
PPSO	d_{ar}	$a_{absorber}$	$d_{IR\ reflector}$	Mi	IA	0.966429236025082
	0.04857568	0.04577764	0.1207137	0.34011779	5	

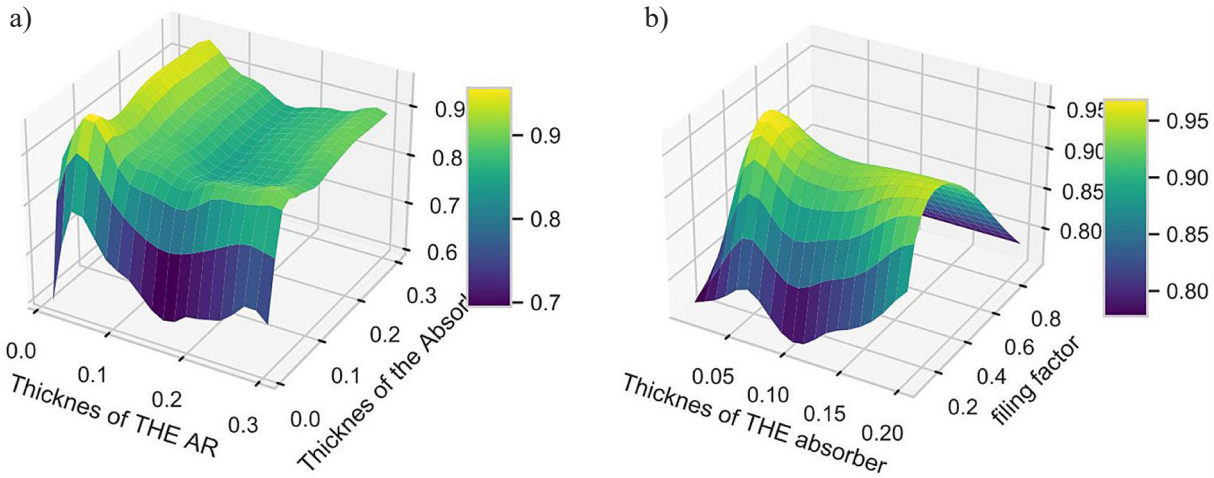

Figure 10. Variation of the absorption α(θ) of the SSA depending on (a) $d_{Absorber}$ & d_{AR}, (b) $d_{Absorber}$ & metal volume fractions variation

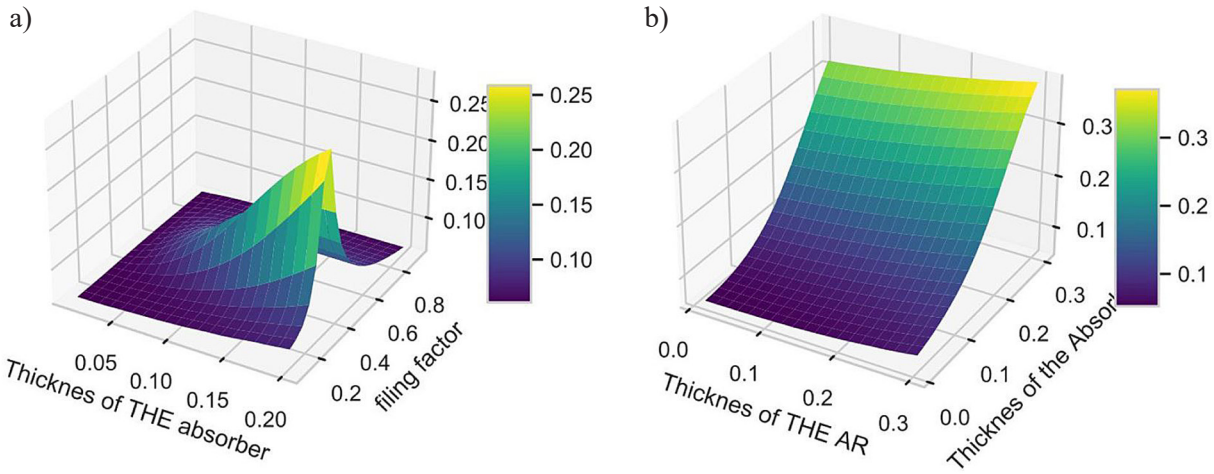

Figure 11. Variation of the absorption ε (θ, T) efficiency of the SSA depending on (a) $d_{Absorber}$ & d_{AR}; (b) $d_{Absorber}$ & metal volume fractions

the cermet layer. Under specific conditions, destructive interference may take place, contingent upon the thickness and optical characteristics of the cermet layer. This utilization of destructive interference in cermet layers that incorporate solar selective absorbers serves to boost the absorption of sunlight and enhance the effectiveness of solar thermal collectors and selective solar absorbers. The careful manipulation and design of the optical features and thickness of the cermet layer are instrumental in achieving this outcome.

Hemisphere cutting

Drawing upon our understanding of nature and our quasi-optical cavity, we notice a weakening trend as the angle of incidence increases. To simplify our calculations, we've divided our hemisphere into five distinct regions, as depicted in Figure 10. As we progressively adjust the apparatus, resolution improves, gradually bringing us closer to achieving a hemispherical shape.

Each segmented portion of our divided hemisphere encounters solar intensity at a specific angle of incidence due to its orientation. It's worth noting that solar intensity reaches its zenith at solar noon, marking the peak of solar energy during the day. Each section possesses a normal vector that intersects with the incidence vector at an angle. Leveraging our advanced algorithmic tool, we aim to optimize each individual section to operate at its maximum efficiency based on its unique conditions and positioning. In essence, we are compelling the environment to adapt to the precise parameters required for each alteration. In the alternative approach, we select individual sections of the hemisphere, each facing the solar radiation at a perpendicular angle. However, these sections experience varying intensities. Specifically, at the highest point, the intensity is 1000 W/m^2, but it diminishes as a function of the cosine of the angle (Cosθ). Our goal is to fine-tune each section to operate in accordance with the specific intensity it receives, as illustrated in Figure 12a.

Table 4 and Figure 18 and 19 present the outcomes derived from our optimized parameters. They illustrate how these parameters interact with the solar intensity curve and are standardized against black body radiation at 100 °C. Additionally, we've included the values of the objective function, representing photo-thermal efficiency, for each scenario. Upon closer examination, we observe that when optimizing based on intensity

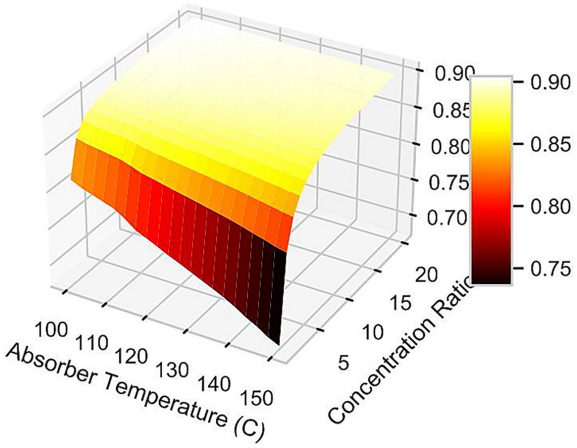

Figure 12. Variation of the $\eta_{solar-th}$ efficiency of the SSA depending on T_a absorber temperature concentration ratio C

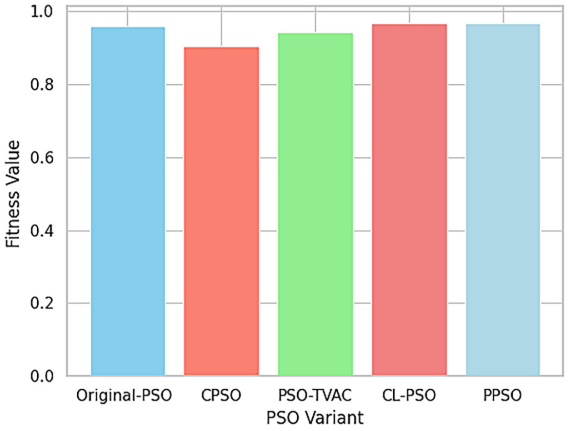

Figure 13. Bar plot of the fitness function values of all adjusted PSO algorithm

initially, the reflective responses across scenarios are nearly identical. This suggests that there may be no need for an intensity-based optimization, as the parameters can remain consistent throughout the entire hemisphere. When discussing the optimization of dependence on the incidence angle, a wide range of results in the reflection curve exists, depending on the chosen algorithm and the method used within the Transfer Matrix Method (TMM). It is observed that as the angle of incidence increases, photothermal conversion decreases. Additionally, with an increase in the thickness of the initial anti-reflective layer and the presence of metallic inclusions, certain physical insights can be derived. To ensure that the system maintains the maximum value even under unfavorable conditions, the construction of a

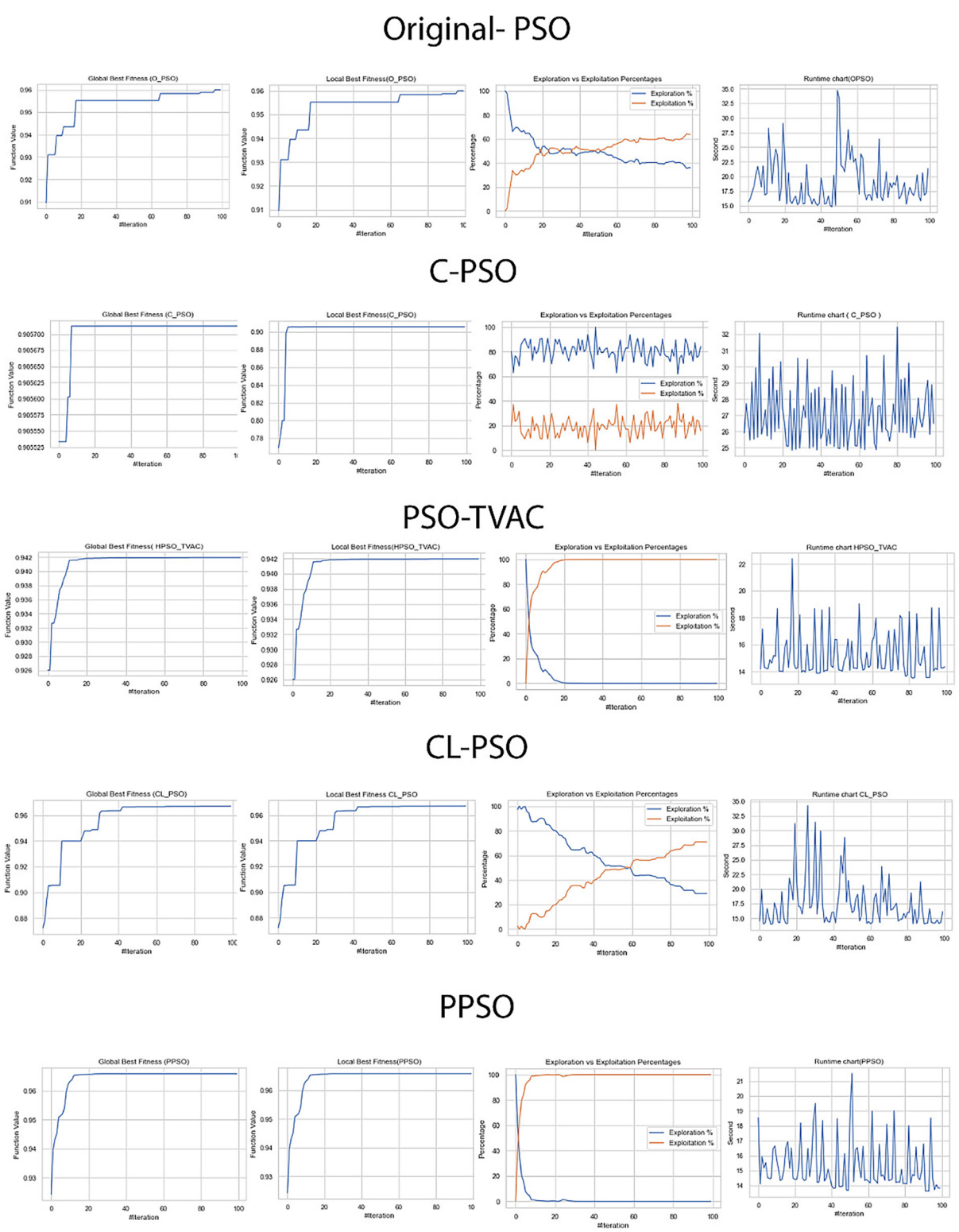

Figure 14. Variation throughout the iterations of global best fitness, local best fitness, exploration vs exploitation and running time

quasi-optical cavity facilitates various absorption processes. These processes include thin film interference and the plasmonic absorption of metal nanoparticles in the cermet layer. As the W filling factor progressively increases, the cermet layer eventually exhibits metallic characteristics due to the abundant contact points between the metal nanoparticles and the dielectric matrix. This interference phenomenon aligns with wave behavior principles. When incident light waves penetrate

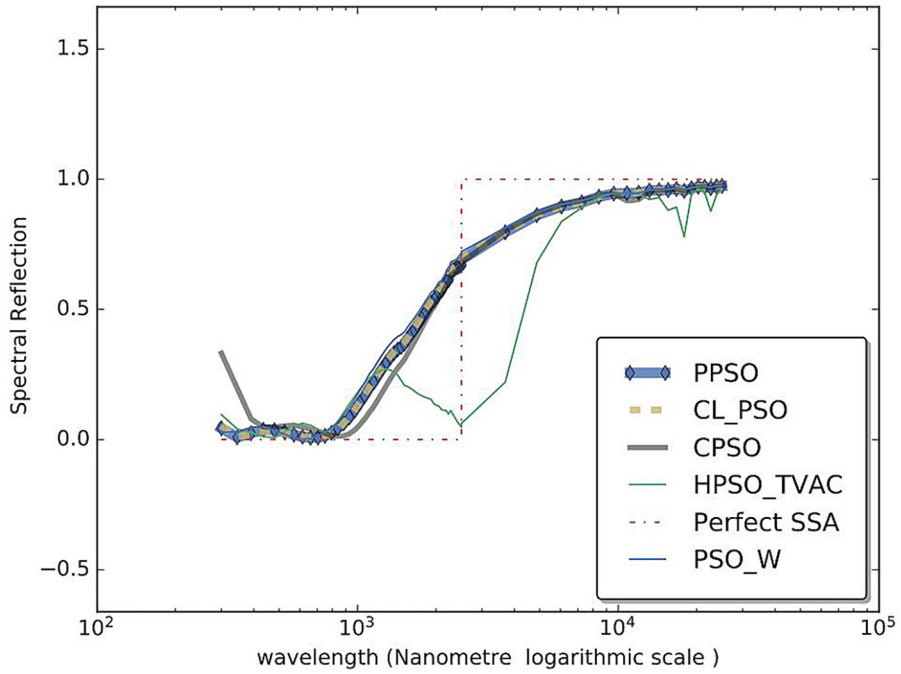

Figure 15. The reflection response of all PSO variants

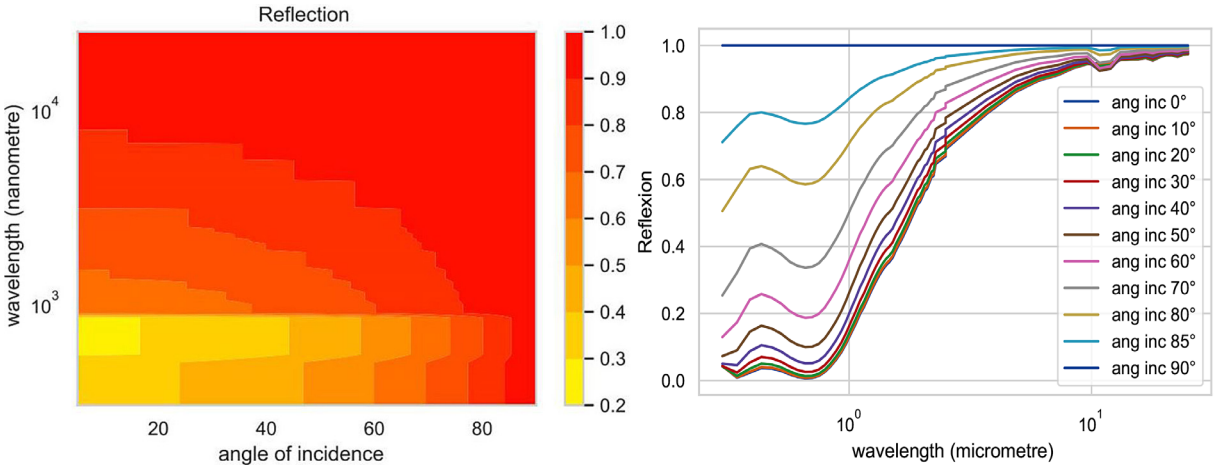

Figure 16. The angular dependence and contour plot of the configuration obtained by the PPSO algorithm

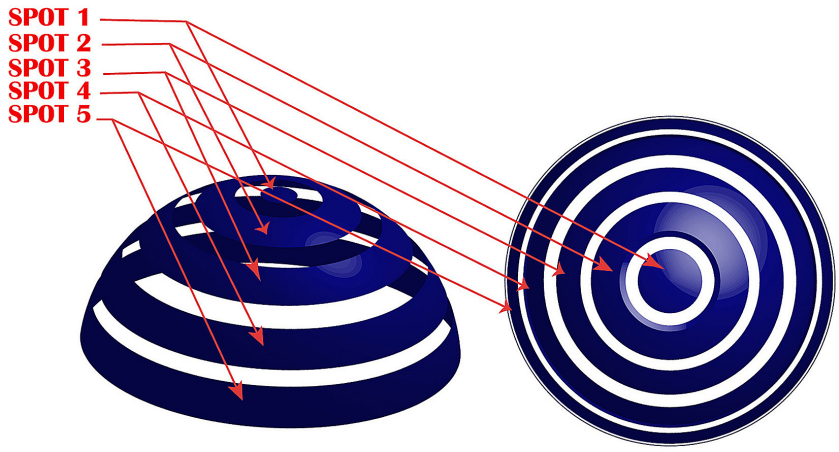

Figure 17. Side view and TOP of the division of the hemisphere into 5 spots

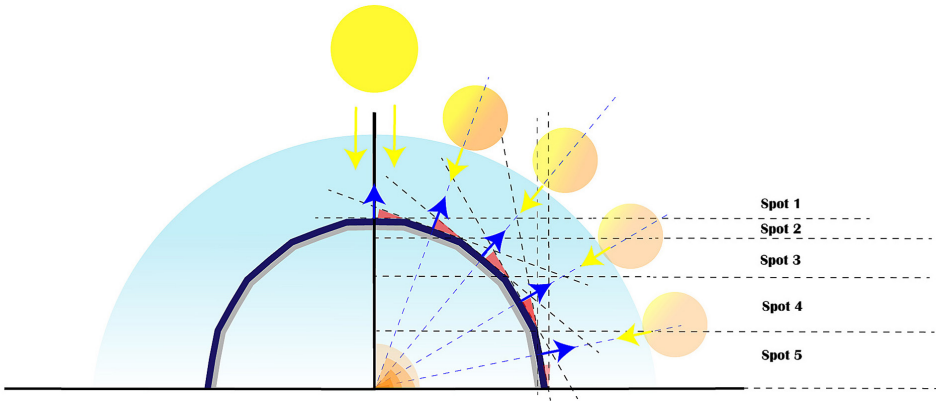

Fig. 18. Different spots, separated by an inclination angle, under the intensity of solar radiation

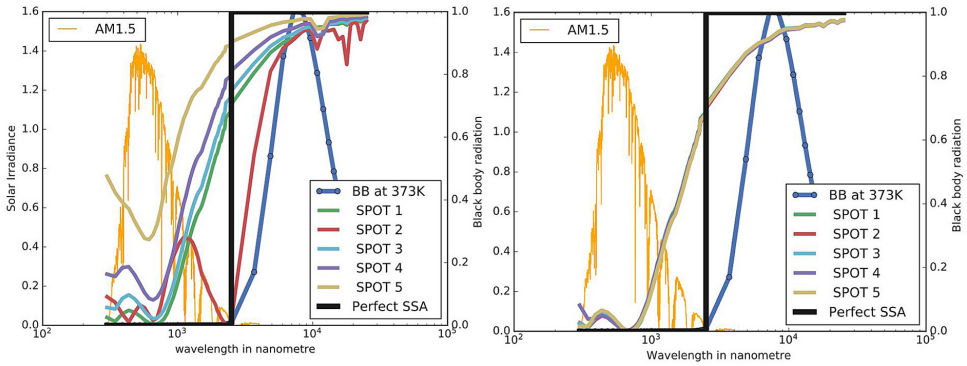

Fig. 19. (a) The reflection response of the 5 spots optimized based on solar noon intensity and its incidence (b) the reflection response of the 5 spots optimized based on solar intensity at each time of the day

Table 4. Displays the optimized values, which are contingent on the angle and intensity dependencies

	Wide angle optimization in I_0 = 1000 Wm /h				Intensity optimization declining by: I_0. cosθ			
SPOT 1	Angle of incidence		Maximum fitness		Normal incidence for intensity 587.7852522924732, fitness: 0.8825094721409645			
	0°		0.9195675879897598					
	d_1	d_2	d_3	Mi	d_1	d_2	d_3	Mi
	0.05125295	0.04322843	0.12730751	0.32684268	0.05125295	0.04322843	0.12730751	0.32684268
SPOT 2	Angle of incidence		Maximum fitness		Normal incidence for intensity 951.0565162951535, fitness: 0.9153571560040987			
	18°		0.8601962354230555					
	d_1	d_2	d_3	Mi	d_1	d_2	d_3	Mi
	0.05125295	0.04322843	0.12730751	0.32684268	0.04781872	0.04519396	0.08847654	0.32309252
SPOT 3	Angle of incidence		Maximum fitness		Normal incidence for intensity 809.0169943749474, fitness: 0.906897481624558			
	36°		0.8884230221379892					
	d_1	d_2	d_3	Mi	d_1	d_2	d_3	Mi
	0.05125295	0.04322843	0.12730751	0.32684268	0.04817211	0.0456218	0.06359603	0.31065172
SPOT 4	Angle of incidence		Maximum fitness		Normal incidence for intensity 587.7852522924732, fitness: 0.8825094721409645			
	54°		0.8146187867950535					
	d_1	d_2	d_3	Mi	d_1	d_2	d_3	Mi
	0.05578856	0.04060122	0.13144161	0.3393818	0.04696187	0.04422857	0.06505458	0.31233323
SPOT 5	Angle of incidence		Maximum fitness		Normal incidence for intensity, fitness: 0.7984328640053393			
	72°		0.600136271293207					
	d_1	d_2	d_3	Mi	d_1	d_2	d_3	Mi
	0.0612712	0.03497301	0.03962809	0.40075995	0.045658	0.045658	0.16292848	0.29783571

the thin film, they undergo multiple interfaces, leading to the interference of reflected waves. Consequently, the primary function of the anti-reflective layer is to mitigate the extent of sunlight reflection from the surface. Its enhanced performance at oblique angles indicates its proficiency in minimizing reflections, even when sunlight approaches at an inclined angle.

We can address this issue and optimize absorption under oblique incidence by simply adding more layers to enhance the phenomenon of destructive interference. This has been demonstrated in the work by Wu et al. (2022), where the addition of extra layers allows for performance that can tolerate absorption angles of up to 80°. However, it's important to note that this approach does complicate the manufacturing process. Nevertheless, the introduction of additional layers offers the potential to achieve performance levels suitable for absorption angles of up to 80°, even though our application operates at a mid-temperature 100–200 °C.

CONCLUSION

In this study, we aimed to enhance the performance of an interfacial solar steam generator designed for water distillation applications. We introduced an innovative hemispherical solar selective absorber, which utilizes a 2D flat plate distributed on a lattice grid shell. Our approach involved optimizing a thin film stack of Al_2O_3/W-Al_2O_3/W using the Phasor Particle Swarm Algorithm. We compared our results with various PSO variants, which allowed us to identify critical parameter values for maximizing photothermal conversion. Notably, our observations revealed superior performance at near-normal angles of incidence.

To further improve our absorber's performance, we implemented a novel approach of dividing the hemisphere into five different spots. Each spot was treated as a flat selective absorber and optimized based on its location within the hemisphere, considering the received intensity and the angle of incidence. While the intensity results remained almost invariant across spots, we observed some variation in the angle of incidence. However, this variation was relatively small, especially for oblique incidences, particularly in areas located at the base during solar noon. To continue enhancing our absorber's performance, we plan to explore the addition of extra layers to increase destructive interference, addressing limitations observed at higher incidences. This research serves as a foundational step for future investigations focused on practical applications in diverse solar regions on Earth, with a special emphasis on the MENA region.

REFERENCES

1. Ajdad, H., Filali Baba, Y., Al Mers, A., Merroun, O., Bouatem, A., Boutammachte, N. 2019. Particle swarm optimization algorithm for optical-geometric optimization of linear fresnel solar concentrators. Renewable Energy, 130, 992–1001. https://doi.org/10.1016/j.renene.2018.07.001
2. Cai, H., Sun, Y., Liu, J., Wang, X. 2021. Genetic algorithm optimization for highly efficient solar thermal absorber based on optical metamaterials. Journal of Quantitative Spectroscopy and Radiative Transfer, 271, 107712. https://doi.org/10.1016/j.jqsrt.2021.107712
3. Chen, J., Li, X., Chen, Y., Zhang, Z., Yu, Y., He, X., Chen, H., Yang, J., Zhang, Z., Yao, X. 2023. Temperature Self-Adaptive Ultra-Thin Solar Absorber Based on Optimization Algorithm. Photonics, 10(5), 546. https://doi.org/10.3390/photonics10050546
4. Chen, L.-Y. (Éd.). 2021. Optical Properties of Solar Absorber Materials and Structures. Springer Singapore, 142. https://doi.org/10.1007/978-981-16-3492-5
5. Duffie, J. A., Beckman, W. A. (s. d.). Solar Engineering of Thermal Processes.
6. Freitas, D., Lopes, L. G., Morgado-Dias, F. 2020. Particle Swarm Optimisation : A Historical Review Up to the Current Developments. Entropy, 22(3), 362. https://doi.org/10.3390/e22030362
7. Ghasemi, M., Aghaei, J., Hadipour, M. 2017. New self-organising hierarchical PSO with jumping time-varying acceleration coefficients. Electronics Letters, 53(20), 1360–1362. https://doi.org/10.1049/el.2017.2112
8. Ghasemi, M., Akbari, E., Rahimnejad, A., Razavi, S. E., Ghavidel, S., Li, L. 2019. Phasor particle swarm optimization : A simple and efficient variant of PSO. Soft Computing, 23(19), 9701–9718. https://doi.org/10.1007/s00500-018-3536-8
9. Grosjean, A., Soum-Glaude, A., Neveu, P., Thomas, L. 2018. Comprehensive simulation and optimization of porous SiO2 antireflective coating to improve glass solar transmittance for solar energy applications. Solar Energy Materials and Solar Cells, 182, 166–177. https://doi.org/10.1016/j.solmat.2018.03.040
10. Grosjean, A., Soum-Glaude, A., Thomas, L. 2021.

Influence of operating conditions on the optical optimization of solar selective absorber coatings. Solar Energy Materials and Solar Cells, 230, 111280. https://doi.org/10.1016/j.solmat.2021.111280

11. Li, Y., Lin, C., Huang, J., Chi, C., Huang, B. 2021. Spectrally Selective Absorbers/Emitters for Solar Steam Generation and Radiative Cooling-Enabled Atmospheric Water Harvesting. Global Challenges, 5(1), 2000058. https://doi.org/10.1002/gch2.202000058
12. Lin, A., Sun, W. 2018. Multi-Leader Comprehensive Learning Particle Swarm Optimization with Adaptive Mutation for Economic Load Dispatch Problems. Energies, 12(1), 116. https://doi.org/10.3390/en12010116
13. Liu, B., Wang, C., Bazri, S., Badruddin, I. A., Orooji, Y., Saeidi, S., Wongwises, S., Mahian, O. 2021. Optical properties and thermal stability evaluation of solar absorbers enhanced by nanostructured selective coating films. Powder Technology, 377, 939–957. https://doi.org/10.1016/j.powtec.2020.09.040
14. Liu, J., Dou, C., Chen, W., Ma, W.-Z., Meng, D., You, X.-Q., Chen, Y.-S., Huang, P.-H., Gu, Y. 2022. Inverse design a patternless solar energy absorber for maximizing absorption. Solar Energy Materials and Solar Cells, 244, 111822. https://doi.org/10.1016/j.solmat.2022.111822
15. Luo, T., Young, R., Reig, P. (s. d.). Aqueduct Projected Water Stress Country Rankings.
16. Ma, W., Chen, W., Li, D., Liu, Y., Yin, J., Tu, C., Xia, Y., Shen, G., Zhou, P., Deng, L., Zhang, L. 2023. Deep learning empowering design for selective solar absorber. Nanophotonics, 12(18), 3589–3601. https://doi.org/10.1515/nanoph-2023-0291
17. Ning, Y., Wang, J., Ou, C., Sun, C., Hao, Z., Xiong, B., Wang, L., Han, Y., Li, H., Luo, Y. 2020. NiCr–MgF2 spectrally selective solar absorber with ultrahigh solar absorptance and low thermal emittance. Solar Energy Materials and Solar Cells, 206, 110219. https://doi.org/10.1016/j.solmat.2019.110219
18. Pyone, E. C., Van, T. H., Le, T. M., Bui, L. V. H. (s. d.). Phasor particle swarm optimization of dome structures under limited natural frequency conditions.
19. Van Thieu, N., Mirjalili, S. 2023. MEALPY : An open-source library for latest meta-heuristic algorithms in Python. Journal of Systems Architecture, 139, 102871. https://doi.org/10.1016/j.sysarc.2023.102871
20. Wang, Z.-Y., Hu, E.-T., Cai, Q.-Y., Wang, J., Tu, H.-T., Yu, K.-H., Chen, L.-Y., Wei, W. 2020. Accurate Design of Solar Selective Absorber Based on Measured Optical Constants of Nano-thin Cr Film. Coatings, 10(10), 938. https://doi.org/10.3390/coatings10100938
21. Wu, Z., Ren, Z., Wang, J., Hou, S., Liu, Y., Zhang, Q., Mao, J., Liu, X., Cao, F. 2022. Realization of an efficient wide-angle solar selective absorber via the impedance matching. Solar Energy Materials and Solar Cells, 238, 111582. https://doi.org/10.1016/j.solmat.2022.111582
22. Xia, X., Li, S. 2020. Research on Improved Chaotic Particle Optimization Algorithm Based on Complex Function. Frontiers in Physics, 8, 368. https://doi.org/10.3389/fphy.2020.00368
23. You, K., Lin, J., Meng, D., Ma, W., Cheng, Y., Liu, J., Deng, X., Chen, Y. 2023. Study of a perfect solar absorber from the visible to the near-infrared band using particle swarm optimization. Optical Materials Express, 13(3), 656. https://doi.org/10.1364/OME.484225
24. Younis, O., Hussein, A. K., Attia, M. E. H., Rashid, F. L., Kolsi, L., Biswal, U., Abderrahmane, A., Mourad, A., Alazzam, A. 2022. Hemispherical solar still : Recent advances and development. Energy Reports, 8, 8236–8258. https://doi.org/10.1016/j.egyr.2022.06.037
25. Yu, H., Liu, D., Duan, Y., Yang, Z. 2015. Applicability of the effective medium theory for optimizing thermal radiative properties of systems containing wavelength-sized particles. International Journal of Heat and Mass Transfer, 87, 303–311. https://doi.org/10.1016/j.ijheatmasstransfer.2015.04.013
26. Zhang, J., Wang, C., Shi, J., Wei, D., Zhao, H., Ma, C. 2022. Solar Selective Absorber for Emerging Sustainable Applications. Advanced Energy and Sustainability Research, 3(3), 2100195. https://doi.org/10.1002/aesr.202100195
27. Zhang, W.-W., Qi, H., Yu, Z.-Q., He, M.-J., Ren, Y.-T., Li, Y. 2021. Optimization configuration of selective solar absorber using multi-island genetic algorithm. Solar Energy, 224, 947–955. https://doi.org/10.1016/j.solener.2021.06.059